Nonlinear evolution of viscoplastic film flows down an inclined plane

Djibrilla Mounkaila Noma, S. Dagois-Bohy, Séverine Millet, Hamda Ben Hadid, Valéry Botton, Daniel Henry

Non-linear evolution of viscoplastic film flows down an inclined plane

Djibrilla Mounkaila Noma[1*], Simon Dagois-Bohy[1*], Séverine Millet[1], Hamda Ben Hadid[1], Valéry Botton[1], Daniel Henry[1]

[1]Univ Lyon, CNRS, Université Claude Bernard Lyon 1, École Centrale Lyon, INSA Lyon, LMFA UMR 5509, Ecully, F-69134, France.

*Corresponding author(s). E-mail(s): djibrilla.mounkaila-noma@univ-lyon1.fr; simon.dagois-bohy@univ-lyon1.fr;

Abstract

In this article, we experimentally investigate the non-linear behavior of a viscoplastic film flow down an inclined plane. We focus on the non-linear instabilities that appear as roll waves. Roll waves are generated by perturbing a permanent flow of Herschel-Bulkley fluid (Carbopol 980) at low frequencies. To determine the local thickness of the film, we used a laser sensor and a camera to globally capture the transverse shape of the waves. For a regular forcing, the results show the existence of different regimes. First, we observe primary instabilities below the cut-off frequency at the entrance of the channel. After the exponential growth of the wave in the linear regime, we recognize the non-linear dynamics with the existence of finite amplitude waves. This finite amplitude depends on the frequency, the Reynolds number and the inclination angle. The results show that this instability is supercritical. At moderate Reynolds numbers, the finite 2-D waves become sensitive to transverse perturbations, due to a secondary instability, and become 3-D waves. The experimental results illustrate a phenomenology of viscoplastic film flows similar to Newtonian fluids, except for the capillary waves.

Keywords: Thin Films, Roll Waves, Non-linear Evolution, Viscoplastic Fluids, Non-Newtonian Fluids, Saturated Amplitude Waves.

1 Introduction

Small perturbations in a gravity-driven flow can lead to the formation of roll waves that travel faster than the bulk flow [1]. Roll waves are a frequent phenomenon in many geophysical flows such as mud, debris or lava flows [2, 3]. As noted by Kohler *et al.* [4], roll waves must be taken into account in any natural hazard assessment. The study of roll waves is also of interest for some industrial applications such as surface coating [5, 6].

The scenario of appearance of these roll waves can be summarised as follows: first, infinitesimal two-dimensional (2-D) perturbations are amplified exponentially when the flow is linearly unstable, i.e. when the Reynolds number is above a critical value [7]. This only happens when the wavelength is long enough, i.e. when the frequency is below a cut-off frequency. When the amplitude is large enough, non-linearities come into play and the perturbation saturates if its frequency is high enough (γ_1 waves), or not if its frequency is too low (γ_2

waves, or solitary waves) [8]. In both cases, a recirculation flow takes place inside the crest of the high amplitude perturbation, hence the name roll-wave [9]. Finally, at high Reynolds numbers, those non-linear 2-D waves may become unstable to transverse perturbations, leading to the growth of three-dimensional (3-D) waves that can be either synchronous or subharmonic [10].

If this scenario seems well-established when the fluid is Newtonian, this is not necessarily the case for non-Newtonian fluids. Numerical and theoretical studies have been carried out on non-Newtonian fluids. De Oliveira Ferreira et al. [11] found that the roll wave amplitudes and lengths decreased along with the disturbance frequency in viscoplastic fluids, and this seems to be also the case for granular matter [12]. The main experimental focus has been for now on the linear instability threshold, which has been notably measured for granular flows [13], shear-thinning fluids [14], viscoplastic fluids [15–18] and shear-thickening fluids [19], as well as on the shape and form of the fully developed roll wave in viscoplastic fluid [20]. However, few experimental investigations of the types of non-linear regimes have been conducted, at least to our knowledge. In this paper, we will explore experimentally different regimes of non-linear waves that can be obtained with a viscoplastic fluid [21] flowing down a slope, and we will compare them with what has been reported in the literature.

The paper will be organised as follows: in a brief state of the art, we will summarise some of the main findings on non-linear regimes for Newtonian and non-Newtonian fluids; then, we will describe our experimental set-up; finally, we will present our results and discuss the phenomenology observed.

2 State of the art

The literature on non-linear regimes of roll waves is rich, and many different effects have been observed. We will focus here on two key points: first, the two different families of non-linear 2-D waves that can arise, and second, the 3-D destabilisation of saturated waves.

In the literature, two main families of roll waves have been identified for the non-linear dynamics of a Newtonian film flow down an inclined plane [8]. First, near the cut-off frequency, γ_1 waves are characterised by finite amplitude (saturation) and steep fronts. These saturated waves are the result of a supercritical instability. Denner *et al.* [22] suggest two leads to explain the saturation of the amplitude: on the one hand, a reduction in inertia acting on the waves due to the recirculation of fluid within the main wave hump, on the other hand larger pressure gradients due to steeper waves with higher Reynolds number. The second wave family introduced by Chang *et al.* [8] for Newtonian fluids is the family of γ_2 waves, or solitary waves. They would be the result of a subcritical instability, which corresponds generally to a sign change in the third Landau coefficient [22]. For non-Newtonian fluids, theoretical studies have predicted the existence of γ_1 waves for power-law fluids [23, 24], Bingham fluids [25], Herschel-Bulkley fluids [26] or viscoelastic fluids [27]. In particular, Balmforth and Liu [26] found that γ_1 waves were also the result of a supercritical instability, and that they saturate after an exponential growth.

At high Reynolds numbers, saturated 2-D waves become unstable to transverse perturbations, leading to the growth of secondary 3-D instabilities [10]. The first instabilities of this kind that can appear are of two types: subharmonic or synchronous. The synchronous instabilities appear far from the marginal stability curve (Re, f) and maintain the periodicity of the saturated waves. They are characterised by a periodic modulation of the transverse wavelength. This wavelength is very large compared to the film thickness. Closer to the linear stability threshold, subharmonic instabilities may occur, resulting in a train of out-of-phase waves in the shape of herringbone patterns. These patterns are very sensitive to the initial conditions, making them more difficult to observe experimentally [28].
We have not found any study, neither numerical nor experimental, that dealt with the transverse destabilisation of saturated roll waves in non-Newtonian fluids.
After this brief state of the art, we will describe our experimental apparatus.

3 Experimental set-up

Experiments are carried out on a glass channel (2 m $\times$ 0.5 m) with an adjustable angle ϕ in the range $0 - 30°$. The fluid in a tank is driven by a pump

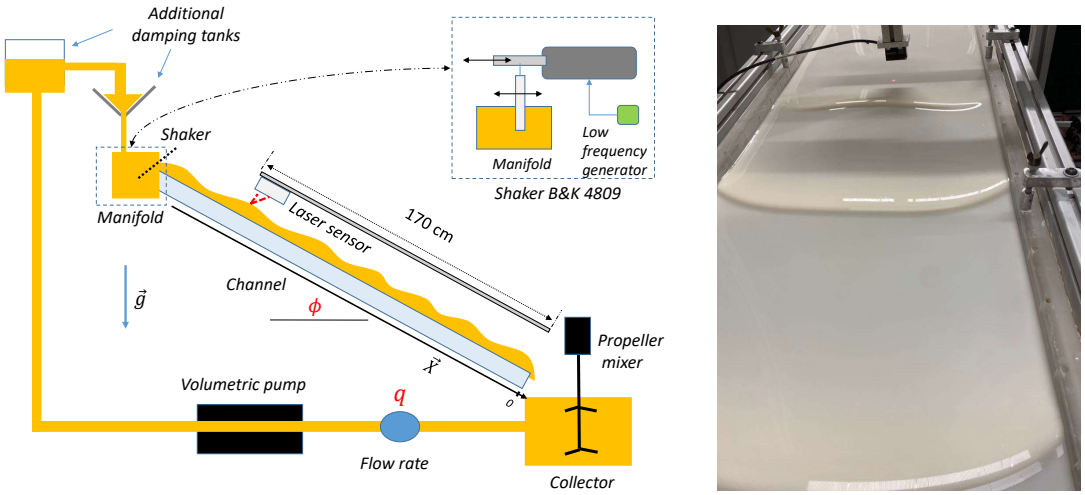

Fig. 1 (Left) Scheme of the experimental set-up inspired from [15]. (Right) A view from above showing an example of disturbed flow: $\phi = 18.2°$; $q = 0.47\ L/s$; $f = 1.5\ Hz$; $\tau_y = 7.42\ Pa$.

PCM EcoMoineau at the entrance of the channel. The flow rate is measured with an electromagnetic flow meter. To mitigate the external disturbance, we have taken great care to install two additional damping tanks with a free surface between the pump and the channel entrance. The experimental set-up (see Fig. 1) is more precisely described in previous works [15, 29]. The longitudinal position $X = 0$ corresponds to the channel outlet.

Our experiments are performed with different Carbopol 980 microgels at neutral pH. For a typical experiment, the fluid was prepared by mixing 100 g of Carbopol powder to 70 L of water. The concentration of Carbopol is approximately 0.14 % in mass. The rheology of the fluids under study is regularly measured with a cone-plate rheometer (LamyRheology Instrument Rheometer RM 200 Touch). The rheological behaviour can be described by the Herschel–Bulkley model:

$$\tau = \tau_y + K\dot{\gamma}^n \ , \qquad (1)$$

where τ_y is the yield stress, K the consistency and n the flow index.

Despite this non-trivial rheological law, Carbopol microgel at sufficiently low concentration remains a simple fluid, in particular thixiotropic and viscoelastic properties can be neglected compared with viscoplasticity [30]. Note that even if Carbopol rheology may be considered simpler than real mud, it can be actually useful to understand various geophysical flows [31, 32]. We added 50 g of titanium dioxide (TiO_2), which corresponds to 0.07 % in mass, to opacify the fluid and allow optical measurements. We verified that the concentration is high enough so that the optical properties do not vary much, but low enough so that the rheological properties differ very little from the pure Carbopol microgel. The TiO_2 particles are too small to see any sedimentation during the experiments.

To create roll waves, the entrance flow rate is perturbed at controlled frequency f and amplitude A at the flow surface (see Fig. 1) using a shaker (B&K 4809) connected to a plate plunging into the entrance manifold. The shaker's displacements are controlled by a low-frequency generator. In this system, the plate is driven and vibrates in the flow direction, generating roll waves. Film thickness h was measured with a laser triangulation sensor (Micro-Epsilon optoNCDT 1420), fixed on a mobile carriage. It works as follows: a laser is shot at the film surface, which creates a bright spot by light diffusion. The distance from this spot to the sensor is measured using triangulation. This allows us to measure the thickness with a precision of 0.01 mm of the film over a region less than 0.5 mm wide. The mobile carriage allows us to measure the local thickness of the film at different positions along the channel, in particular close

to the outlet of the channel, to study the evolution of the wave amplitude. We have also investigated the wave patterns using a Sony E-mount camera placed above the channel.

Adopting the Balmforth and Liu [26] conventions, the dimensionless Reynolds Re and Bingham Bi numbers are given by:

$$Re = \frac{\rho \tan(\phi)}{K} \left(\frac{\rho g \langle h \rangle^{1+n} \sin\phi}{K} \right)^{\frac{2-n}{n}} \langle h \rangle^n \ , \quad (2)$$

$$Bi = \frac{\tau_y}{\rho g \langle h \rangle \sin\phi} \ , \quad (3)$$

with ρ the density, g the gravity and $\langle h \rangle$ the undisturbed film thickness. The Bingham number is defined as the ratio between the yield stress and the maximum viscous shear stress. With our definitions, the term in $cot(\phi)$ is included in the Reynolds number, and the Froude number is related as follows: $Fr^2 = Re$.

The main measurement uncertainties are given in the Table (1). The uncertainty in the flow rate is assessed by comparing the flowmeter measurement with a direct measurement (using a balance).

4 Non-linear evolution

In this section, we focus on the non-linear evolution of the waves measured in about 100 experiments. We first describe the finite amplitude 2-D waves. Next, we present the experimental results on the secondary instabilities.

4.1 Finite amplitude 2-D waves

We will now experimentally analyze the evolution of the wave amplitude along the channel for different frequencies f, flow rate q and inclination ϕ. For this purpose, we have measured the local thickness at different positions along the channel using the laser sensor. The peak-to-peak amplitude A is obtained by the difference between the maximum and minimum thicknesses over a given period.

For an unsteady flow, Fig. 2(a) shows that the waves amplitude increases linearly at the entrance of the channel and then reaches a finite constant. The roll-waves generation depend on the length of the channel, as indicated by Di Cristo *et al.* [33]. This saturation is accompanied by steep fronts, similar to those shown in Fig. 2(b) with time signals at four different positions along the channel (90, 50, 10 and 0 cm from the channel outlet). Note that we obtain the same amplitude at $X = -10$ cm and $X = 0$ cm as the waves have reached saturation amplitude.

We have modeled the evolution of waves amplitude with a Landau equation in order to determine the kind of instability that develops:

$$\frac{dA}{dX} = \sigma A - \frac{l}{2} A^3 \ , \quad (4)$$

where A is the wave amplitude, σ the linear wave growth rate, X the longitudinal position and l the Landau coefficient. In the example shown in Fig. 2, a linear growth rate of 0.047 cm^{-1} was first obtained from the amplitude variation in Fig. 2(a). Then, we calculated the Landau coefficient l by plotting $\sigma A - \frac{dA}{dX}$ according to A^3 in Fig. 3. We found a constant slope $l/2 = 0.104$, which shows that the instability is supercritical since $l > 0$. In fact, for $l > 0$, the effective growth rate $\left(\sigma - \frac{l}{2} A^2 \right)$ decreases as the wave amplitude increases, which leads to a finite amplitude. These waves seem to correspond to the γ_1 family waves described in the literature [8, 28] for Newtonian fluids, which occur as a supercritical instability characterized by a finite amplitude.

Fig. 4 shows that the finite amplitude increases as the Reynolds number (flow rate) increases (see Fig. 4(b)) and/or the frequency decreases (see Fig. 4(a)). Theses observations are qualitatively in agreement with the simulations of viscoplastic fluid [11, 26] and power-law fluid [23].

To understand these observations, we propose a model in which the saturated finite amplitude regime corresponds to the situation where all the fluid within a wavelength is driven along by the wave. Estimating that the volume of fluid under a wave varies as A_f^2, if there is no loss and the waves have not been accelerated, this volume must correspond to the volume initially contained over a period such that:

$$A_f \sim \sqrt{\lambda(\langle h \rangle - h_p)} \sim \sqrt{\frac{c}{f}(\langle h \rangle - h_p)} \ , \quad (5)$$

where A_f is the wave finite amplitude, λ the wavelength, $\langle h \rangle$ the average film thickness, f the

Table 1 Summary of measurement errors.

Variables	Absolute errors	Relative errors	Evaluation method
Inclination ϕ	0.1°	0.3 - 0.7 %	Minimum graduation
Flow rate q	5.3 mL/s	1.2 %	Direct measurement
Amplitude wave A	10 μm	0.1 - 1 %	Sensor measurement error

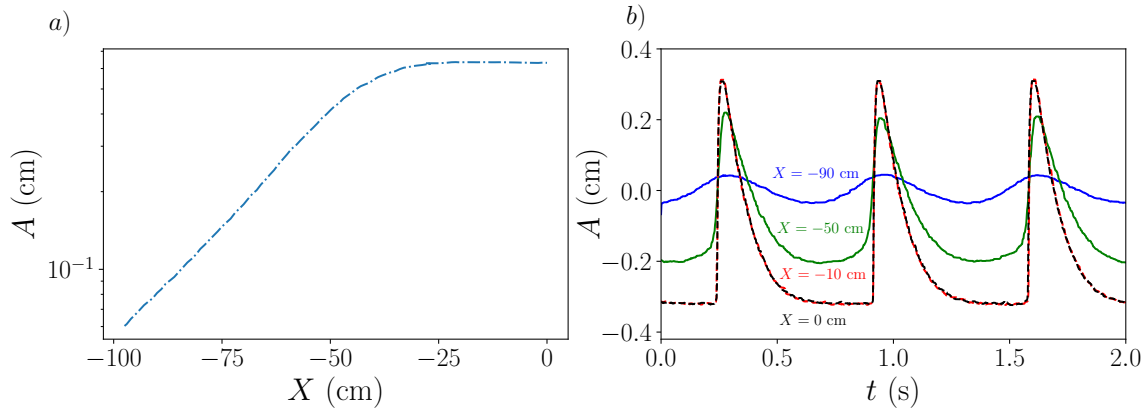

Fig. 2 a) Evolution of waves amplitude depending on the position X along the channel for a viscoplastic film ($\tau_y = 1.34$ Pa, $K = 1$ Pa.s^n, $n = 0.53$, $\phi = 13.9°$, $q = 0.396$ L/s, $f = 1.5$ Hz , $\langle h \rangle = 0.47$ cm). b) Temporal evolution of the wave amplitude at 4 different positions X from the outlet, respectively (blue) $X = -90$ cm, (green) $X = -50$ cm, (red) $X = -10$ cm and (black) $X = 0$ cm. The position $X = 0$ corresponds to the channel outlet. The evolution at $X = -10$ cm and $X = 0$ cm are similar as the waves have reached saturation amplitude.

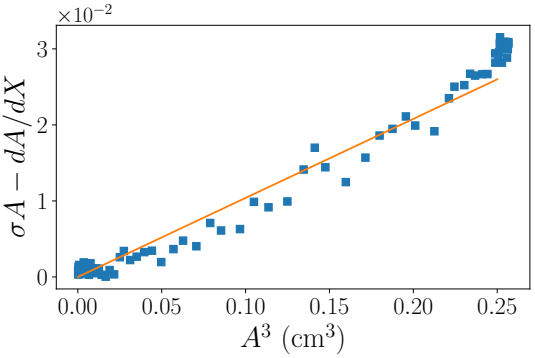

Fig. 3 $\sigma A - \frac{dA}{dX}$ as a function of A^3 for viscoplastic film flow (the same case as Fig. 2). The blue squares correspond to the experimental data and the line is a linear fit.

frequency, h_p the pseudo-plug thickness and c the phase speed. We used Balmforth and Liu [26] results for c and h_p. Fig. 5(a) shows for two different flow configurations a good agreement between the experimental data and this model concerning the decrease of the wave finite amplitude as a function of the frequency, as observed in a numerical model in [11].

Fig. 5(b) shows the waves finite amplitude normalised by the average film thickness as a function of the Reynolds number Re. Initially, an increase in Re causes an increase of amplitude at the outlet of the channel. Then, the normalized amplitude seems to reach a maximum. This observation is consistent with the literature for Newtonian fluids [22] and viscoplastic fluids [20].

Table 2 Linear spatial growth rate σ, waves finite amplitude A_f and Landau coefficient l according to frequency for the cases in Fig. 4(a).

f (Hz)	1.2	1.4	1.6	1.8	2	2.2
σ (cm^{-1})	0.041	0.042	0.042	0.040	0.038	0.033
l	0.106	0.127	0.160	0.161	0.178	0.170
A_f (cm)	0.752	0.705	0.677	0.655	0.630	0.573

Table 2 gives the variation of the waves finite amplitude and the Landau coefficient with the disturbance frequency for the cases studied in Fig. 4(a). It shows that the Landau coefficient decreases at low frequencies and that the sign change of the Landau coefficient in order to get a

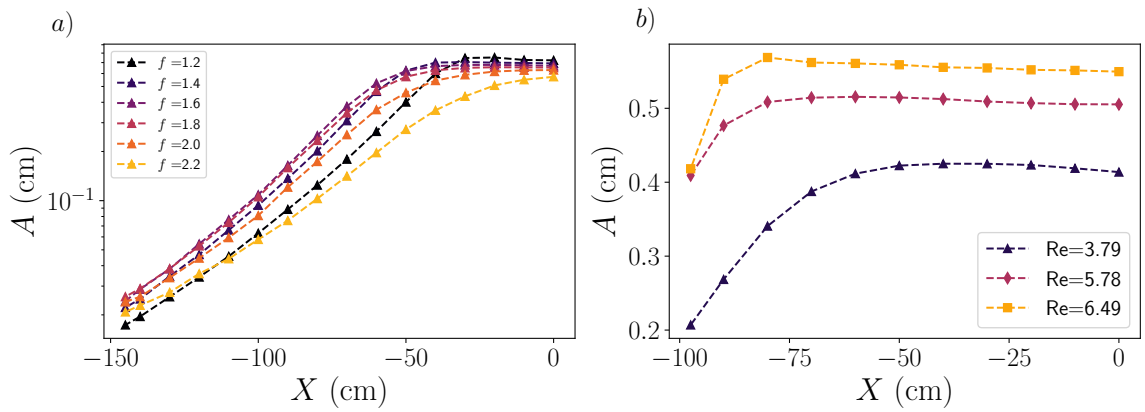

Fig. 4 Waves amplitude in a viscoplastic film flow down an inclined plane as a function of the position X: a) for different disturbance frequencies with $\tau_y = 2.44$ Pa, $K = 0.66$ Pa.s^n, $n = 0.55, \phi = 15.6°$, $q = 0.400$ L/s and $\langle h \rangle = 0.41$ cm; b) for different Re with $\tau_y = 1.34$ Pa, $K = 1$ Pa.s^n, $n = 0.53$, $\phi = 13.9°$ for a frequency $f = 1.7$ Hz.

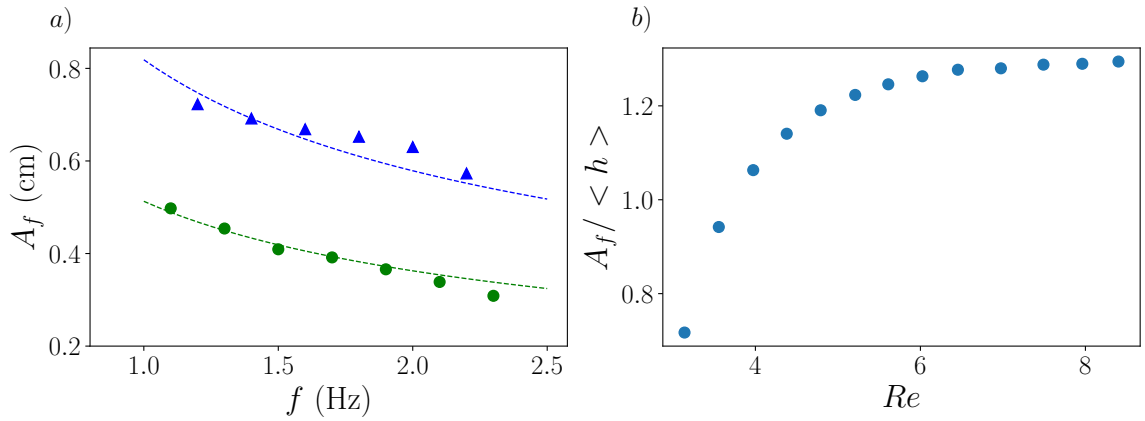

Fig. 5 a) Experimental waves finite amplitude as a function of the disturbance frequency for two cases. In blue triangles, the case described in Fig. 4(a) and in green circles, a film flow with $\tau_y = 2.03$ Pa, $K = 0.59$ Pa.s^n, $n = 0.58$, $\phi = 13.2°$, $q = 0.204$ L/s, $\langle h \rangle = 0.36$ cm. The lines are the predictions obtained with the model (5). b) Waves finite amplitude normalised by the average film thickness $A_f/\langle h \rangle$ as a function of Re for the case described in Fig. 4(b).

subcritical instability should then take place for a frequency lower than 1 Hz. Below this frequency however, the response of the shaker is poor, which probably explains the difficulty we had in observing solitary waves similar to those of the γ_2 wave family [28] obtained for Newtonian fluids. Furthermore, it is not obvious that they exist for viscoplastic fluids, due to yield stress.

4.2 Secondary instabilities

As mentioned in section (2), for Newtonian fluids, the saturated 2-D waves may become unstable to transverse perturbations, leading to the growth of 3-D instabilities: synchronous or subharmonic, respectively far from and near the marginal stability curve. We have investigated the wave patterns for a viscoplastic film flow to determine whether the waves remain 2-D as in Fig. 1, or not. We want to emphasise that this destabilisation is progressive along the flow, and the ability to observe it is likely to depend on the length of the channel.

Using a camera placed above the end of the channel, we studied the stability diagram in the (Re, f) plane with two inclination angles ($\phi = 26.9°$ and $\phi = 30.6°$), and we reported if the flow observed there was 2-D or 3-D, as shown in Fig. 6. For each diagram, we have two areas. First, an area above the marginal curve where the flow is stable, and second an area below the marginal

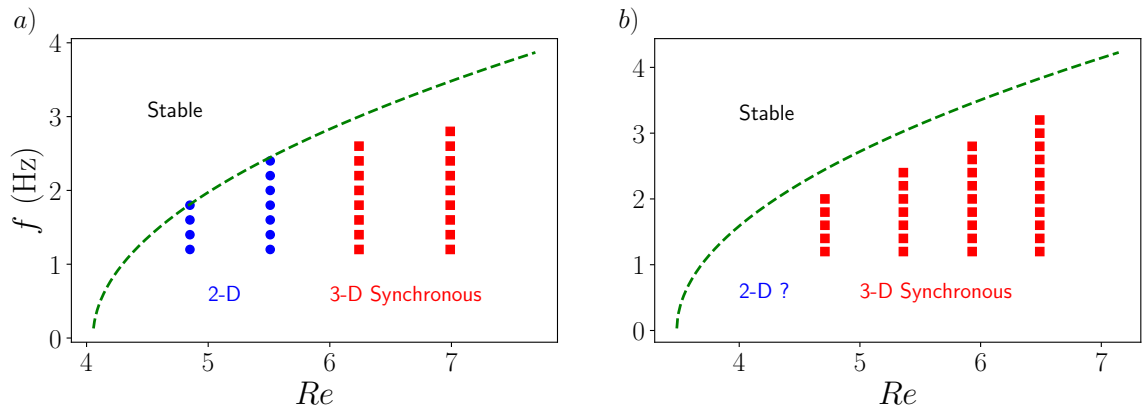

Fig. 6 Stability diagram in the (Re, f) plane for a) $\phi = 26.9°$ and b) $\phi = 30.6°$ with $\tau_y = 5$ Pa, $K = 2.3$ Pa.s^n, $n = 0.5$. The green line corresponds to the marginal curve, the blue points (respect. red squares) give the parameter sets where 2-D waves (respect. 3-D waves) are observed. A rescaled diagram in the (Re, St) plane is available as supplementary material with the Strouhal number $St = f\langle h\rangle/V$.

curve where it is unstable. The marginal curve was obtained using the methodology of Mounkaila Noma *et al.* [15].

At an inclination $\phi = 26.9°$, Fig. 6(a) shows that at low Reynolds numbers, the waves remain 2-D and then become 3-D as the Reynolds number increases. An example of such a destabilisation is shown Fig 7. At $\phi = 30.6°$, we observed only 3-D waves at the end of the channel, as reported in Fig. 6(b), and Fig. 8 represents some wave patterns captured at this angle. Note that below $Re = 4.71$, the amplitude of the roll waves is too small to determine their type. We find that the destabilisation patterns are similar to those observed in the literature [10, 28]. The wavefront shape is modulated by a transverse sine of low amplitude compared to the longitudinal wavelength (see Fig. 8). At first sight, the 3-D waves exhibit a much larger transverse wavelength than what is observed in Newtonian fluids. However, this is still consistent if we note that this transverse wavelength is similar in magnitude to the main longitudinal wavelength, as it is for the synchronous instabilities in Newtonian fluids. Unfortunately, we could not observe any subharmonic waves. The first reason is simply that they appear close to the marginal curve, where the growth rates are very low and the waves get out of the channel before they could destabilise. The second reason could be the high sensitivity of these asynchronous waves to the initial conditions, as explained by Scheid *et al.* [28]. Nevertheless, our experiments illustrate the influence of the inclination angle in the development of instabilities, and our observations are similar to those in the work of Liu *et al.* [10] for Newtonian fluids and the simulations of Miladinova *et al.* [23] for power-law fluids.

Finally, at moderate angle and low Re, we observed the appearance of instabilities with a rivulet-like pattern, that is when the center crest is accelerated and seems not bounded anymore with the rest of the wavefront. This results in a gradual and inhomogeneous modification of the wavelength, the effect being more pronounced at low frequency (see Fig. 9). Rivulets have been observed also in Newtonian fluids [34], but usually at much higher angles, when the plate is near-vertical, and, often, dewetting processes are involved. Here, the angles are much lower and surface tension plays no apparent role, therefore we believe it could be a new kind of destabilisation, made possible by the change of rheology.

5 Conclusion and perspective

In this paper, we present experiments with Carbopol microgel aiming at studying the non-linear dynamics of a viscoplastic film flow down an inclined plane. Through the improvement of a previous set-up [15], this set-up allows to investigate the wave amplitude along the channel (2 m × 0.5 m). Hence, we report finite amplitude waves similar to the γ_1 family waves for Newtonian fluids

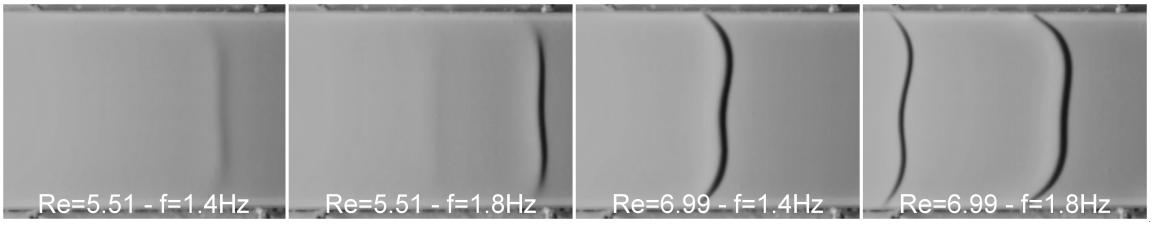

Fig. 7 Wave patterns observed experimentally at $\phi = 26.9°$ for the case in Fig. 6(a). The two-dimensional waves at low Re become three-dimensional at moderate Re.

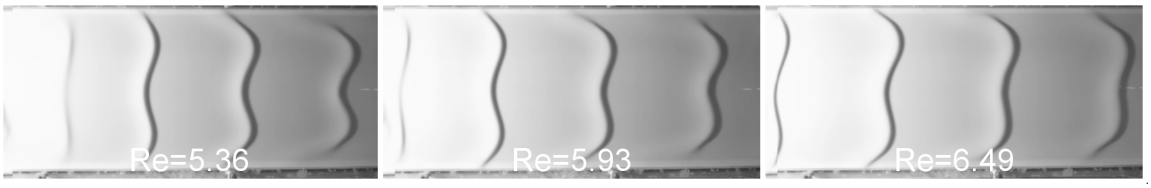

Fig. 8 Wave patterns observed experimentally at $f = 2$ Hz and $\phi = 30.6°$ for the case in Fig. 6(b). The wavefront is similar to three-dimensional synchronous instabilities [10, 28] for Newtonian fluids.

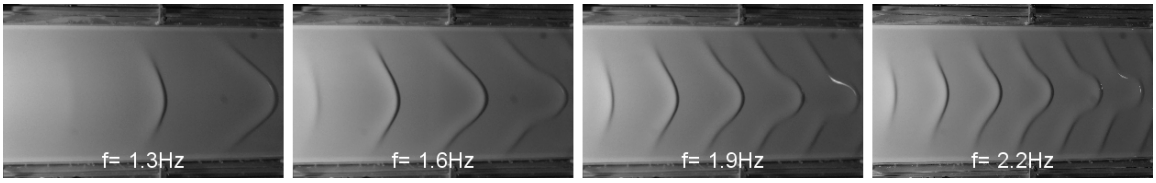

Fig. 9 Wave patterns observed experimentally with $\phi = 23.5°$, $\tau_y = 3.4$ Pa, $K = 0.98$ Pa.s^n, $n = 0.56$ and $Re = 0.86$.

[8]. Theses waves are the result of a supercritical instability and characterized by steep fronts. We observe that the finite amplitude increases as Re increases and/or the frequency decreases. We also show that, after an increase of amplitude at the channel outlet with Re, the amplitude normalized by the average film thickness $A_f/\langle h \rangle$ seems to reach a maximum. These observations are in agreement with the simulations of Balmforth and Liu [26] for viscoplastic fluids and Denner *et al.* [22] for a glycerol solution. Finally, our study shows the appearance of secondary instabilities affecting the finite amplitude waves. By increasing the slope of the incline, we note the appearance of 3-D synchronous instabilities [10, 28]. These results illustrate the destabilising role of Re and ϕ on the flow dynamics. However, we were unable to observe capillary waves and 3-D subharmonic instabilities. The evolution of the 3-D non-linear waves remains to be explored in more details.

Acknowledgements

We thank S. Martinez and G. Geniquet for their assistance building the experimental set-up.

Declaration

Data availability

The datasets generated and analysed during the current study are available from the corresponding author on reasonable request.

Declaration of interests

The authors report no conflict of interest.

Author Contributions

The authors confirm contribution to the paper as follows: conceptualization, methodology and data collection: DMN and SDB; analysis, interpretation of results and writing: DMN, SDB and SM; supervision, discussion and critical review: HBH, DH and VB.

Funding

No funding was received for conducting this study.

References

[1] R.F. Dressler, Mathematical solution of the problem of roll-waves in inclined open channels. Communications on Pure and Applied Mathematics **2**(2-3), 149–194 (1949). https://doi.org/10.1002/cpa.3160020203

[2] F. Engelund, W. Zhaohui, Instability of hyperconcentrated flow. Journal of Hydraulic Engineering **110**(3), 219–233 (1984). https://doi.org/10.1061/(ASCE)0733-9429(1984)110:3(219)

[3] C. Ancey, Plasticity and geophysical flows: A review. Journal of non-Newtonian Fluid Mechanics **142**(1), 4–35 (2007). https://doi.org/10.1016/j.jnnfm.2006.05.005. Viscoplastic fluids: From theory to application

[4] A. Köhler, J. McElwaine, B. Sovilla, M. Ash, P. Brennan, The dynamics of surges in the 3 february 2015 avalanches in vallée de la sionne. Journal of Geophysical Research: Earth Surface **121**(11), 2192–2210 (2016). https://doi.org/10.1002/2016JF003887

[5] P.J. Cheng, K.C. Liu, C.C. Wang, in *Applied Mechanics and Materials*, vol. 479 (Trans Tech Publ, 2014), pp. 45–49. https://doi.org/10.4028/www.scientific.net/AMM.479-480.45

[6] D.J. Dhas, A. Roy, Wavy regime of a colloidal falling film. Physical Review Fluids **7**(6), 064307 (2022). https://doi.org/10.1103/PhysRevFluids.7.064307

[7] J. Liu, J.D. Paul, J.P. Gollub, Measurements of the primary instabilities of film flows. Journal of Fluid Mechanics **250**, 69–101 (1993). https://doi.org/10.1017/S0022112093001387

[8] H.C. Chang, E. Demekhin, D. Kopelevich, Nonlinear evolution of waves on a vertically falling film. Journal of Fluid Mechanics **250**, 433–480 (1993). https://doi.org/10.1017/S0022112093001521

[9] N. Kofman, S. Mergui, C. Ruyer-Quil, Three-dimensional instabilities of quasi-solitary waves in a falling liquid film. Journal of Fluid Mechanics **757**, 854–887 (2014). https://doi.org/10.1017/jfm.2014.506

[10] J. Liu, J. Schneider, J.P. Gollub, Three-dimensional instabilities of film flows. Physics of Fluids **7**(1), 55–67 (1995). https://doi.org/10.1063/1.868782

[11] F. de Oliveira Ferreira, G.d.F. Maciel, J.B. Pereira, Roll waves and their generation criteria. RBRH **26** (2021). https://doi.org/10.1590/2318-0331.262120200185

[12] J. Gray, A. Edwards, A depth-averaged-rheology for shallow granular free-surface flows. Journal of Fluid Mechanics **755**, 503–534 (2014). https://doi.org/https://doi.org/10.1017/jfm.2014.450

[13] Y. Forterre, O. Pouliquen, Long-surface-wave instability in dense granular flows. Journal of Fluid Mechanics **486**, 21–50 (2003). https://doi.org/10.1017/S0022112003004555

[14] M.H. Allouche, V. Botton, S. Millet, D. Henry, S. Dagois-Bohy, B. Güzel, H. Ben Hadid, Primary instability of a shear-thinning film flow down an incline: experimental study. Journal of Fluid Mechanics **821**, R1–R11 (2017). https://doi.org/10.1017/jfm.2017.276

[15] D. Mounkaila Noma, S. Dagois-Bohy, S. Millet, V. Botton, D. Henry, H. Ben Hadid, Primary instability of a visco-plastic film down an inclined plane: experimental study. Journal of Fluid Mechanics **922**, R2 (2021). https://doi.org/10.1017/jfm.2021.528

[16] A. Tamburrino, C.F. Ihle, Roll wave appearance in bentonite suspensions flowing down inclined planes. Journal of Hydraulic Research **51**(3), 330–335 (2013). https://doi.org/10.1080/00221686.2013.769468

[17] M. Arai, J. Huebl, R. Kaitna, Occurrence conditions of roll waves for three grain–fluid models and comparison with results from

experiments and field observation. Geophysical Journal International **195**(3), 1464–1480 (2013). https://doi.org/10.1093/gji/ggt352

[18] C. Zhao, M. Zhang, T. Zhang, F. Wang, et al., Response of roll wave to suspended load and hydraulics of overland flow on steep slope. Catena **133**, 394–402 (2015). https://doi.org/10.1016/j.catena.2015.06.010

[19] B. Darbois Texier, H. Lhuissier, Y. Forterre, B. Metzger, Surface-wave instability without inertia in shear-thickening suspensions. Communications Physics **3**(1), 232 (2020). https://doi.org/10.1038/s42005-020-00500-4

[20] G.d.F. Maciel, F.d.O. Ferreira, E. Cunha, G. Fiorot, Experimental apparatus for roll-wave measurements and comparison with a 1d mathematical model. Journal of Hydraulic Engineering **143**(11), 04017046 (2017). https://doi.org/10.1061/(ASCE)HY.1943-7900.0001366

[21] N.J. Balmforth, I.A. Frigaard, G. Ovarlez, Yielding to stress: recent developments in viscoplastic fluid mechanics. Annual Review of Fluid Mechanics **46**, 121–146 (2014). https://doi.org/10.1146/annurev-fluid-010313-141424

[22] F. Denner, A. Charogiannis, M. Pradas, C.N. Markides, B.G. Van Wachem, S. Kalliadasis, Solitary waves on falling liquid films in the inertia-dominated regime. Journal of Fluid Mechanics **837**, 491–519 (2018). https://doi.org/10.1017/jfm.2017.867

[23] S. Miladinova, G. Lebon, E. Toshev, Thin-film flow of a power-law liquid falling down an inclined plate. Journal of non-Newtonian Fluid Mechanics **122**(1-3), 69–78 (2004). https://doi.org/10.1016/j.jnnfm.2004.01.021

[24] C. Ruyer-Quil, S. Chakraborty, B. Dandapat, Wavy regime of a power-law film flow. Journal of Fluid Mechanics **692**, 220–256 (2012). https://doi.org/10.1017/jfm.2011.508

[25] P.J. Cheng, H.Y. Lai, Finite-amplitude long-wave instability of Bingham liquid films. Nonlinear Analysis: Real World Applications **10**(3), 1500–1513 (2009). https://doi.org/10.1016/j.nonrwa.2008.01.018

[26] N. Balmforth, J. Liu, Roll waves in mud. Journal of Fluid Mechanics **519**, 33–54 (2004). https://doi.org/10.1017/S0022112004000801

[27] Q.F. Fu, T. Hu, L.J. Yang, Instability of a weakly viscoelastic film flowing down a heated inclined plane. Physics of Fluids **30**(8), 084102 (2018). https://doi.org/10.1063/1.5041494

[28] B. Scheid, C. Ruyer-Quil, P. Manneville, Wave patterns in film flows: modelling and three-dimensional waves. Journal of Fluid Mechanics **562**, 183–222 (2006). https://doi.org/10.1017/S0022112006000978

[29] D. Mounkaila Noma, Stabilité d'un film viscoplastique sur un plan incliné. Thèse, Université de Lyon (2021). URL https://tel.archives-ouvertes.fr/tel-03663371

[30] J. Piau, Carbopol gels: Elastoviscoplastic and slippery glasses made of individual swollen sponges: Meso-and macroscopic properties, constitutive equations and scaling laws. Journal of non-Newtonian Fluid Mechanics **144**(1), 1–29 (2007). https://doi.org/10.1016/j.jnnfm.2007.02.011

[31] E. Di Giuseppe, F. Corbi, F. Funiciello, A. Massmeyer, T. Santimano, M. Rosenau, A. Davaille, Characterization of carbopol® hydrogel rheology for experimental tectonics and geodynamics. Tectonophysics **642**, 29–45 (2015). https://doi.org/10.1016/j.tecto.2014.12.005

[32] P. Freydier, G. Chambon, M. Naaim, Experimental characterization of velocity fields within the front of viscoplastic surges down an incline. Journal of non-Newtonian Fluid Mechanics **240**, 56–69 (2017). https://doi.org/10.1016/j.jnnfm.2017.01.002

[33] C. Di Cristo, M. Iervolino, A. Vacca, On the applicability of minimum channel length criterion for roll-waves in mud-flows. Journal of Hydrology and Hydromechanics **61**(4),

286–292 (2013). https://doi.org/10.2478/johh-2013-0036

[34] S. Alekseenko, S. Aktershev, A. Bobylev, S. Kharlamov, D. Markovich, Nonlinear forced waves in a vertical rivulet flow. Journal of Fluid Mechanics **770**, 350–373 (2015). https://doi.org/10.1017/jfm.2015.170